47th AIAA Aerospace Sciences Meeting Including The New Horizons Forum and Aerospace Exposition
5 - 8 January 2009, Orlando, Florida

Linear Stability Study of Hypersonic Boundary Layer Transition on Blunt Circular Cones

Jia Lei * and Xiaolin Zhong†
University of California, Los Angeles, California 90095

A linear stability analysis is conducted to investigate hypersonic flows over blunt circular cones with a Mach 5.5 free-stream. The flow conditions are chosen to be the same as those of Stetson's boundary layer transition experiments performed in 1967. The transition reversal phenomenon with respect to the nose bluntness was first observed by Stetson in these experiments. Therefore, the purpose of this study is to investigate the effects of nose bluntness on the linear stability of the boundary layer. For the case that transition reversal was observed experimentally, the second mode N factor is found to be too small to trigger the transition at the location reported in the experiment. The results show no bluntness induced reversal effects based on the second mode growth. In addition, another case adapted to Stetson's Mach 8 experiment in 1984 is studied to investigate the second mode characteristics under different flow conditions.

1. INTRODUCTION

Extensive wind-tunnel and flight-test experiments on boundary layer transition and a number of stability experiments have been conducted for hypersonic flows over circular cones [1,2] in the last fifty years. Recently, Schneider [1,2] did a comprehensive review on the existing experiments and flight-testing reports. Though many of these experiments did not measure the transition mechanisms and were conducted in noisy wind tunnels, these experiments have led to better understanding of the effects on transition of many parameters, including nose bluntness, Mach number, surface and stagnation temperatures, freestream unit Reynold numbers, cone half angle and angle of attack, etc. Nevertheless, so far, the influences from these parameters on transition still remain unclear.

Stetson et al. [5, 6] carried out boundary-layer stability experiments on an axisymmetric blunt cone in a Mach 7.99 free stream. Detailed fluctuation spectra of the disturbance waves developing along the body surface were measured. It was found that the disturbances in the boundary layer were dominated by the second mode instability. Significant super harmonic components of the second modes were observed after the second mode became dominant. Compared with similar hypersonic flow over sharp cone, the second mode instability of the blunt cone appeared in much further downstream location. This indicates a stabilization of the boundary layer by slight nose bluntness. Stetson et al. [3] also carried out shock tunnel investigation of boundary layer transition at Mach 5.5. The half angle of the cones is 8 degrees.

* Graduate Student, Mechanical and Aerospace Engineering Department.
† Professor, Mechanical and Aerospace Engineering Department. Associate Fellow, AIAA. xiaolin@seas.ucla.edu

A number of nose radii were used in the test ranging from 0.03125 inch to 0.5 inch as shown in fig.1. If arranging those transition data reported by Stetson [3] for a number of cones with different nose radiuses and flow conditions, one can generate a plot of free-stream transition Reynolds number versus free-stream Reynolds number based on nose radius as shown in fig.2. The figure shows clearly the transition reversal start from free-stream Reynolds number based on nose radius about 3×10^5, which falls into the category of "large" nose bluntness. No DNS or e^N calculations have been done on this case to confirm the reversal effects. The nose bluntness effects was further studied by Stetson in [5]. Stability experiments of hypersonic flows over sharp or blunt cones have also been carried out by other researchers. Demetriades [7, 8] did extensive stability experiments on hypersonic boundary layers over axisymmetric cones. Recently, Maslov and his colleagues [9, 10] reported their stability experiments on supersonic and hypersonic flows over sharp and blunt cones.

The normal mode linear stability characteristics of the boundary-layer flow over the same blunt cone as Stetson et al.'s experiments [6] have been studied by a number of researchers: imcluding Malik et al. [11], Herbert et al. [12], Kufner et al. [13, 14], Rosenboom et al. [15], Lyttle et al. [16], and Zhong [17]. Malik et al. [11] computed the neutral stability curve and compared the growth rates obtained by LST with the experimental results. The steady base flow solution was computed by using the parabolized Navier-Stokes equations. They found that the nose bluntness stabilizes the boundary layer. The growth rates predicted by the LST were compared with Stetson et al.'s experimental results at the surface location of s = 175 nose radii (0.667 m). The linear stability analyses predicted slightly lower frequency for the dominant second mode, but much higher amplification rates than the experimental results.

Rosenboom et al. [15] did further study on the effect of nose bluntness on the linear stability of hypersonic flow over Stetson's blunt cone. In their studies, the cone geometry and freestream conditions were adapted to the Stetson's experiments. Three cases of blunt cones of different nose radius, which cover both ``small'' and ``large'' bluntness, were considered. The purpose was to investigate, by linear stability analysis, the transition reversal phenomenon observed in experiments at ``large'' bluntness [4]. By a linear stability analysis, Rosenboom et al. confirmed a monotonic downstream movement of the second mode critical Reynolds number as nose radius increases. However, their linear stability analysis still cannot explain the transition reversal phenomena observed in experiment at ``large'' bluntness. Their results indicated that there is a need for better understanding of boundary layer receptivity as well as nonlinear transition phenomena for engineering transition predication.

The linear stability theory has been used and proven successful in analyzing the instability of hypersonic boundary layer. In this paper, the focus is placed on the hypersonic flow over the blunted cones. By far, many researchers have studied the laminar-turbulent transition on blunted cones through experiments and numerical analysis. Some general trends on the effect of nose bluntness had been understood based on their studies. As concluded by Malik *et al*. [11] and Rosenboom *et al*. [15], the nose bluntness effect substantially stabilized the flow fluctuation and delayed the transition compared with the sharp cones. Moreover, as the nose bluntness increase, the initiation of transition will move further downstream until some critical bluntness is reached. A further increment in nose bluntness after reaching the critical value of nose bluntness will lead to a phenomenon called "transition reversal'. The mechanism of the transition reversal is

mysterious and has not been completely understood. Different researchers proposed different theories to explain this reversal, but none of them have been fully accredited.

Even though lots of experiments have been conducted on hypersonic flow over blunt cones, most of them lack essential information to interpret the instability mechanism and flow behavior. Through the numerical study and linear stability analysis, we believe we can have a better understanding on the missing pieces of information. In order to have a more complete picture on the study of laminar-turbulent transition of hypersonic flow over blunt cone, in the current report, we will mainly study the hypersonic flow over blunt circular cone with the flow conditions adapted to those of Stetson's experiment reported in 1967. The effect of nose bluntness, free-stream Mach number, surface temperature treatment, unit Reynolds number and cone half-angle will be investigated. The linear stability theory (LST) will be applied to analyze the second mode instability of disturbance waves inside the boundary layer. The N factor of the semi-empirical e^N method will also be carried out to correlate with the experimental transition data. Also, another case with flow conditions adapted to Stetson's experiment in 1984 is studied to understand the influence of flow conditions to the stability characteristics.

2. GOVERNING EQUATIONS AND NUMERICAL METHODS

2.1 The Base Flow

The governing equations and numerical method for the base flow computation are briefly stated in this section. Details derivation and numerical method for three-dimensional axisymmetric flow had been described in previous papers (Zhong [31,32]). The governing equations are the unsteady three-dimensional Navier-Stokes equations written in the following conservative form:

$$\frac{\partial U^*}{\partial t^*}+\frac{\partial F_j{}^*}{\partial x_j{}^*}+\frac{\partial F_{vj}{}^*}{\partial x_j{}^*}=0 \tag{1}$$

where $U^*=(\rho^*,\rho^* u_1^*,\rho^* u_2^*,\rho^* u_3^*,e^*)$, and superscript "*" represents dimensional variables. The Cartesian coordinates are denoted by (x_1^*,x_2^*,x_3^*) in tensor notation. In the current simulation of axisymmetric flow over blunt cones, x^* is along the centerline of the cone toward the downstream direction. The origin of coordinate is located at the center of spherical nose. The flow velocities are non-dimensionlized by the free-stream velocity U_∞^*, similarly, the length, density, pressure, temperature and time are non-dimensionlized by $r_n^*,\rho_\infty^*,p_\infty^*,T_\infty^*$ and r_n^*/U_∞^*, etc. The dimensionless variables are presented by dropping the superscript "*".

A fifth-order shock-fitting method by Zhong [28] is used to compute the flow field bounded by the bow shock and cone surface. The flow variables behind the shock are determined by Rakine-Hugoniot relations across the shock and a characteristic compatibility equation behind the shock.

2.2 The Linear Stability of Axisymmetric Disturbance

The linear stability theory (LST) is applied to study the instability of hypersonic flow over blunt cones in this report. Based on the LST, the disturbances are limited to small amplitude. In hypersonic regime, the dominant instabilities, the Mack's second mode is found to be most amplified along the stream-wise direction. Hence, the normal mode of disturbances is assumed to have the following form:

$$q' = \hat{q}(y_n) e^{i(-\omega t + \alpha s)} \tag{2}$$

In the above equation, q' can be any flow variable such as velocity, temperature, density and pressure. And $\hat{q}$ is the eigenfunction of the variable representing the complex amplitude of the disturbance. In the spatial stability theory, ω, the dimensionless angular frequency of a normal disturbance mode , is a real number. $\alpha = \alpha_r + \alpha_i$ is the stream-wise direction wave number, which is a complex value. The imaginary part of wave number is the spatial growth rate of a specific disturbance mode. When α_i turns negative, the disturbance becomes unstable. The real part of wave number α_r represents the spatial wave number of disturbance. An important quantity that can be derived from it is the non-dimensional phase velocity, which is defined as:

$$a = \frac{\omega}{\alpha_r} = \frac{FR}{\alpha_r} \tag{3}$$

In the above equation, the dimensionless phase velocity is normalized by the free-stream velocity. F is dimensionless frequency such that

$$F = \frac{\omega^* \upsilon_\infty^*}{U_\infty^{*2}} \tag{4}$$

R is local Reynolds number based on the length scale of boundary layer thickness:

$$R = \frac{\rho_\infty^* U_\infty^* L^*}{\mu_\infty^*}, \text{ where } L^* = \sqrt{\frac{\mu_\infty^* s^*}{\rho_\infty^* U_\infty^*}} \tag{5}$$

And s^* is the curvilinear coordinate along the cone surface measuring from the nose tip.

Similarly, the dimensional wave number and growth rate are related to their corresponding dimensionless quantities by the following equations:

$$\alpha_r^* = \frac{\alpha_r}{\sqrt{s^* \upsilon_\infty^* / U_\infty^*}} \tag{6}$$

$$\alpha_i^* = \frac{\alpha_i}{\sqrt{s^* \upsilon_\infty^* / U_\infty^*}} \tag{7}$$

One of the most common applications of LST analysis in predicting the laminar-turbulent is the N factor calculation based on a semi-empirical method called e^N method. According to this method, the transition will occur when the amplification of amplitude of the disturbances reach certain critical level. The ratio of the change amplitude of disturbance with fixed frequency can be calculated as they travel downstream. Since the growth rate is not a constant, the amplitude ratio between two locations can be expressed as an integral:

$$e^N = \frac{A}{A_0} = \exp \int_{s_0^*}^{s^*} \frac{1}{A} \frac{dA}{ds} ds^* \tag{8}$$

Or, just for the N factor,

$$N = \int_{s_0^*}^{s^*} -\alpha_i^* ds^* \tag{9}$$

In the integral, s_0^* corresponds to the location that the disturbance just turns neutrally stable. By the integration, the amplification in amplitude of a specific disturbance as it moves downstream can be evaluated. On the other hand, the N factor leading to transition is determined from the experimental measurement. The transition N factor is not fixed for all the cases. It does depend on the flow conditions, object geometry and other unknown parameters. Even under the same flow conditions, the N factor differs when different unstable modes are considered. Here, the different unstable modes refer to the Mack's first mode and second mode. In general, the N factor of first mode is smaller than the one of second mode. For high Mach number flow (Ma>4), the second mode is most dominant unstable mode, so the N factor calculated in this paper is reported sorely for second mode instability waves.

3. TEST CASES and FLOW CONDITIONS

Many wind tunnel and flight tests have been conducted on hypersonic boundary layer transition over blunt circular cones [1, 2]. We will conduct further studies on two of the cases shown in *table 1* [3, 6].

Case 1: (Stetson's 1984 experiment)
$M_\infty = 7.99$ $\quad \mathrm{Re}_\infty = 8.78\times10^6\ m^{-1}$
Cone half angle: 7°
$P_t^* = 4\times10^6\ Pa$ $\quad T_t^* = 750K$
Wall temperature: adiabatic wall temperature
nose radius: r= 3.81 mm, r=42.67 mm
Case 2: (Stetson's 1967 experiment)
$M_\infty = 5.468$ $\quad \mathrm{Re}_\infty = 18.95\times10^6\ m^{-1}$
Cone half angle: 8°

$P_\infty^* = 7756.56\,Pa$ $\quad\quad$ $T_t^* = 1227.88K$

Wall temperature: $T_w = 296K$

Nose radius: r=3.969 mm, r=12.7 mm, r=38.1mm

Table 1. Test Cases in the Study of Hypersonic Flow over Blunt Cones

For both the numerical simulation and LST analysis, the ideal gas model is adapted with $\gamma = 1.4$, Prandtl number $Pr = 0.72$ and gas constant $R = 286.94\,Nm/kgK$. Sutherland's law is used to evaluate the viscosity based upon the local temperature.

Case 1 is investigated primarily in the purpose of validation. Also, the effect of nose bluntness is observed by increasing the nose radius with the same flow condition. Case 2 is the major study case of current paper. The transition locations were measured and the transition reversal phenomenon was first reported. The stability study on this specific case helps to gain further understand in the transition process.

4. RESULTS and DISCUSSION

4.1 The Base Flow Computation

The base flows for all the study cases are obtained from the direct numerical simulation performed by Zhong using the method stated in section 2. The CFD code had been tested and validated on many different flow conditions. For all cases, the highly accurate base flow profiles were resulted. The detail discussion of the base flow results are provided by Zhong[33]. Here, sample non-dimensional flow field profiles of case 2 (Stetson's Mach 5.5 case) with nose radius of 3.969 mm are presented. In fig. 3-5, the η is the distance from the body surface normalized by the nose radius.

One feature of hypersonic flow over blunt cone is the presence of entropy layer which will be swallowed further downstream. In Fig. 5, the generalized inflection point due to the entropy layer effect is observed at the location upstream of the transition. The generalized inflection point is the essential condition for the appearance of instability. However, even reported by some researchers [32], the entropy layer instability is not found in the current study.

4.2 LST results of Case 1:

For the validation purpose, the LST calculation was first performed on case 1 which corresponds to the Stetson's experiment in 1984 with 3.81 mm nose radius [6]. The results are compared with those from other researchers.

In fig. 6, the dimensionless growth rates of unstable second mode obtained by current LST calculation at s=175 are shown. In the same figure, the numerical results reported by Malik *et al*. [11] and Herbert and Esfahanian *et al*. [12] are also provided for comparison. All three results agreed rather well in the second mode region. The small discrepancies are mainly due to the fact that the LST calculations are very sensitive to the base flow field. Kufner *et al*. [14] provided a very good discussion on the sensitivity of LST results to the accuracy of the base flow. However, when comparing the first mode behavior, Malik's result predicts a significantly higher growth rate than the current calculations. It is because in the current

calculations, the disturbance waves are restricted to be axisymmetric, while in Malik's calculations, the three-dimensional (asymmetric) waves were taken into account. Therefore, in Malik's results, the first mode growth rates reflected the oblique waves with most unstable growth rates. Since it is believed that for hypersonic flow, the dominant unstable modes are the Mack's second mode, the LST study in this paper mainly focuses on understanding the second mode mechanism.

Other than the unstable second mode, some stable modes were also found. The growth rates and phase velocities of Mack modes together with the stable modes at surface location s=175 were plotted in fig. 7 and fig. 8. For simplicity, the stable modes were named mode I, mode II and mode III, respectively. As shown in Fig. 6, the mode I, mode II and mode III were always stable. It seems that they have nothing to do with the unstable mode at all. However, if their corresponding phase velocities are calculated, as shown in Fig. 7, it is found that whenever the stable and unstable mode intersect, it causes an abrupt change of growth rates for both stable and unstable modes. It turns out that Fig. 7 and Fig. 8 were very useful in understanding the receptivity mechanism of hypersonic boundary layer. Since, receptivity is not the subject of this paper; the detail will be discussed in a separate report by Zhong [33].

By evaluating the growth rates at different locations, a neutral stability curve (fig. 9), can be generated. From this curve, one can clearly identify the disturbance wave at which frequency will become unstable first, and at which Reynolds number it will start to turn unstable. And the Reynolds number just mentioned is called the critical Reynolds number. In this case, the critical Reynolds number is about 1550 and has a frequency corresponding to second mode disturbance. In the study of Rosenboom *et al.* [15], the neutral curve for the three-dimensional disturbance waves is considered. The critical number for first mode and second mode were almost coincided. The critical Reynolds number is correlated to the transition Reynolds number with the latter one further downstream. Therefore, the neutral stability curve can be used to roughly estimate the transition location. But this is not reliable for most engineering applications because it only indicates where the disturbance waves start to grow but not how much they grow.

A more reliable method in predicting the transition is the semi-empirical e^N method. As mentioned in earlier section, in order to perform the calculation using e^N method, the N factor for each fixed frequency can be found by carrying the integration (Eq. 9). In fig. 10, the second mode dimensionless growth rates are plotted against the local Reynolds number. The calculations by Malik *et al.* [11] on the maximum growth rates at each local Reynolds number was compared with the current results. And the current result predicts a slightly higher growth rate than Malik's.

Fig. 10 shows the N factor result for the cone with 3.81mm nose radius. As shown, not all the disturbance frequencies are amplified to the same level. Only some selected frequencies are responsible to the onset of transition. If the empirical N factor for transition is provided, from Fig.10, the range of frequency within which the disturbances will lead to transition can be identified. From the fig. 11, one at least gains some ideas about which range of disturbance frequency is more likely to be responsible for the transition to turbulence. Since Stetson *et al.* [6] did not provided the transition N factor for the current test case, Rosenboom *et al.* [15] assumed it was the same as the sharp cone, which N equals to 4.5. Based on this N factor, the transition

should occur at s^* =0.8 m. However, in the experimental measurement, no transition was observed in this case. It means that the actual transition N factor from experimental measurement is needed in order to interpret the N factor calculations correctly.

Other than the test case with 3.81 mm nose radius, an artificial test case with nose radius of 42.67mm (with no experimental data) is also computed to observe the influence of nose bluntness. For this case, the second mode instability does not emerge until much further downstream. In fig. 12, the second mode dimensional growth rate is found to be barely unstable at location *s* about 6.0 m. Since the base flow is calculated only up to about 6.3 m along the stream-wise direction, no further growth rate data can be obtained. Nonetheless, the result is in a reasonable agreement with Rosenboom's result [15]. The N factor calculation is not performed here due to the insufficiency of data.

4.3 LST Results of Case 2:

Case 2 is the primary study case in this report. The flow conditions of this case are adapted to Stetson's shock tube experiment in 1967 [3]. The LST results of three different nose bluntness are presented, which are r=3.969 mm, r=12.7 mm and r=38.1 mm respectively.

In fig.13-15, the growth rates are plotted versus the downstream location *s*. Some common characteristics are observed in these study cases. The disturbance with higher frequency turns unstable at location closer to the nose tip. As the frequency of the disturbance decrease, the peak of second mode growth rate reaches a maximum value. After that, the peak value gradually decreases. This trend is not observed in fig. 13 because the instabilities spread out in a wide range of surface distance which is not covered in this calculation, but it is clearly showed in the other two cases. For example, on the cone with nose radius of 12.7 mm (fig. 14), the maximum growth rate is about 37 $1/m$ with frequency about 526 KHz.

Another important observation on the influence of bluntness is that blunting the nose forces the second mode instability to squeeze toward the nose tip, as shown in fig. 14 and fig.15. For these two blunter cones, due to the strong non-parallel effect in the region very close to the nose tip, the LST analysis is no longer applicable. Therefore, in the natural stability curve of the second mode (fig.19), the critical Reynolds numbers cannot be determined for the two blunter cones.

Comparing the ranges of frequencies of the unstable second mode of all three cones, it is found that the unstable frequency spectrum shifts toward the lower end as the nose radius increase. In other words, the range of unstable frequencies is selected by the nose radius of cone. Therefore, when conducting the direct numerical simulation studies on each of the above case, different range of disturbance frequencies need to be imposed to effectively simulate the instability mechanism inside the boundary layer of hypersonic flow. An improper choice of disturbance frequencies would produce results reflecting a completely unrealistic model. Hence, the LST analysis is a very powerful tool in identifying the unstable frequency spectrum that is more likely to become dominant in the process of transition. The wave numbers for all the cones studied in Case 2 are presented in fig. 16-18 in order to compare with the DNS results, which will be provided in a separate paper by Zhong [33].

In Stetson's experiment [3], the transition locations were recorded. The transition N factor can be determined by correlating the N factor calculation based on LST analysis with the location of transition from the experiment. Fig. 20-22 show the N factor for three different nose bluntness versus the downstream location. According to the experimental data, for the cone with nose radius of 3.969 mm, the transition occurred at s ≈ 0.406 m. Matching this number on the N factor diagram (fig. 20) gives an N factor about 3. Table 2 lists the transition location from experiment and the corresponding predicted N factor for each of the three cones with different bluntness.

r_n	Free stream Re based on r_n	transition location	Experimental N factor	$R_{,tr}$
3.969 mm	75213	0.406 m	3	2770
12.7 mm	240665	0.421 m	3.2	2823
38.1 mm	721995	0.243 m	1.1	2146

Table 2. Transition Locations and transition N factors of Case 2

The N factor for the first two cones with r = 3.969 mm and r = 12.7 mm are comparable, while the N factor of the bluntest cone, which the transition reversal occurred, appear to be much smaller. The N factor values for all three cones are lower than the conventionally accepted value of the e^N method. The method usually predicts transition with an N factor between 5 and 10. In spite of the inconsistency in the transition N factor, the transition local Reynolds numbers of all blunt cones do not vary dramatically.

4.4 Interaction of Modes for Case 2

It has been understood that the second mode instability is generated by synchronization of a discrete normal mode originates from the fast acoustics wave – mode F and a discrete mode originates from the slow acoustics wave – mode S. Most of the LST studies show that the mode S becomes unstable second mode after the resonance interaction between mode F and mode S. However, in current study, the mode F becomes the second mode instead. Fig. 23 shows the phase speed of mode F and mode S for the cone with nose radius of 3.969 mm at a fixed surface location s=120, it is clearly indicated that, the mode F is coming off the fast acoustic wave with wave speed $1+1/M$. Also, the mode S detaches from the slow acoustics wave with wave speed $1-1/M$. These two modes synchronize at about $\omega = 0.27$. In the vicinity of synchronization, the growth rate of mode F abruptly drops to unstable, while mode S becomes more stable (fig. 24). Away from the synchronization point, the mode F recovers and becomes stable again. The same pattern is observed on the blunter cones. Also, in fig. 25 and 26, the non-dimensional eigenfunctions of unstable second mode at the synchronization point are shown. All the fluctuation structures are clustered at location very close to the surface of the cone body.

4.5 Second mode characteristics under different flow conditions

In the LST analysis, different behaviors of the second mode instabilities are observed on case 1 and case 2. For case 1, as the nose bluntness increases, the appearance of unstable second mode get further delayed. The critical Reynolds number changes from 1550 to about 7000 when the nose radius changes from 3.81mm to 42.67 mm. While, for case 2, increasing the nose radius forces the unstable second mode getting closer and closer toward the nose tip of the cone as

shown in fig. 19. It is believed that the different behaviors on the second mode instabilities are due to the differences of the flow conditions. The obvious difference in these two cases is the wall temperature condition. The wall temperature in case 1 is set to the adiabatic condition. And the wall temperature of case 2 is fixed at 296K, which is much cooler than the wall temperature of case 1. The wall cooling effect will stabilize the first mode and destabilize the second mode. Also, removing heat from flow will cause the boundary layer become thinner. Another important difference is the free stream unit Reynolds number. The case 2 has a unit Reynolds number more than 2 times of the one for the case 1. The implication between the unit Reynolds number and the second mode behavior still remains unclear. However, the LST results imply that the unit Reynolds number might play a crucial role in the transition process.

5. CONCLUSIONS

The Stetson's experiments with a free-stream Mach 5.5 conducted in 1967 are investigated using LST analysis. The growth rate and N factors for a wide range of free stream disturbance frequencies are calculated. The transition N factors are determined by correlating the current N factor calculations with the experimental transition location data. For the case in which the transition reversal was observed, the N factor based upon the second mode growth is found to be about 1.1. The second mode transition N factor is too weak to be the dominant mechanism causing the transition. This implies some other unknown factors that lead to transition reversal are still waiting to be identified.

In addition, by comparing the second mode instabilities in case1 and case 2, it is found that different flow conditions also alter the second mode instabilities significantly. The wall temperature conditions and the free-stream unit Reynolds number are shown to be important in controlling the behavior of second mode.

Acknowledgments

This work was sponsored by the Air Force Office of Scientific Research, USAF , under AFOSR Grant # FA9550-04-1-0029 and #FA9550-07-1-0414, monitored by Dr. John Schmisseur. The views and conclusions contained herein are those of the authors and should not be interpreted as necessarily representing the official policies or endorsements either expressed or implied, of the Air Force Office of Scientific Research or U.S. Government.

References:

1. Schneider, S.P., *Hypersonic Laminar-Turbulent Transition on Circular Cones and Scramjet Forebodies.* Progress in Aerospace Sciences, 2004. 40: p. 1-50.
2. Schneider, S.P., *Flight Data for Boundary-Layer Transition at Hypersonic and Supersonic Speeds.* Journal of Spacecraft and Rockets, 1999. 36(1): p. 8-20.
3. Stetson, K.F.R., G. H., *Shock Tunnel Investigation of Boundary-Layer Transition at M = 5.5.* AIAA JOURNAL, 1967. **5**(5): p. 899-906.
4. Ericsson, L.E., *Effects of Nose Bluntness and Cone Angle on Slender Vehicle Transition.* AIAA Paper 87-1415, 1987.

5. Stetson, K.F., *Nosetip Bluntness Effects on Cone Frustum Boundary Layer Transition in Hypersonic Flow.* AIAA paper 1983-1763, 1983.
6. Stetson, K.F., Thompson, E. R., Donaldson, J. C., and Siler, L. G., *Laminar Boundary Layer Stability Experiments on a Cone at Mach 8, Part 2: Blunt Cone.* 1984. AIAA paper 84-0006.
7. Demetriades, A., *Hypersonic Viscous Flow Over A Slander Cone. Part III: Laminar Instability and Transition.* AIAA paper 74-535, 1974.
8. Demetriades, A., *Laminar Boundary Layer Stability Measurements at Mach 7 Including Wall Temperature Effects.* AFOSR-TR-77-1311, 1977.
9. Maslov, A.A., Shiplyuk, A. N., Sidorenko, A., and Arnal, D., *Leading-edge Receptivity of a Hypersonic Boundary Layer on a Flat Plate.* Journal of Fluid Mechanics, 2001. 426: p. 73-94.
10. Maslov, A.A., Mironov, S. G., Shiplyuuk, A. A., Sidorenko, A. A., Buntin, D. A., and Aniskin, V. M., *Hypersonic Flow Stability Experiments.* 2002. AIAA 2002-0153.
11. Malik, M.R., Spall, R. E., and Chang, C. L., *Effect of Nose Bluntness on Boundary Layer Stability and Transition.* 1990. AIAA Paper 90-0112.
12. Herbert, T.a.E., V., *Stability of Hypersonic Flow over a Blunt Body.* AGARD CP, 1993. 514: p. 28.
13. Kufner, E., Dallmann, U., and Stilla, J., *Instability of Hypersonic Flow Past Blunt Cones - Effects of Mean Flow Variations.* 1993. AIAA paper 93-2983.
14. Kufner, E., and Dallmann, U. *Entropy and Boundary Layer Instabilityof Hypersonic Cone Flows - Effects of Mean Flow Variations*. in *IUTAM Symposium on Laminar-Turbulent Transition*. 1994. Sendai/Japan: Springer-Verlag, Berlin.
15. Rosenboom, I., Hein, S., and Dallmann, U., *Influence of Nose Bluntness on Boundary-Layer Instabilities in Hypersonic Cone Flows* AIAA Paper 99-3591, 1999.
16. Lyttle, I.J.R., H. L.; Shipyluk, A. N.; Maslov, A. A.; Buntin, D. A.; Burov, E. V.; Schneider, S. P., *Numerical-Experimental Comparisons of Second-Mode Behavior for Blunted Cones.* AIAA paper 2004-97, 2004.
17. Zhong, X., *Numerical Simulation and Experimental Comparison of Hypersonic Boundary Layer Instability over a Blunt Cone.* AIAA paper 2004-2244, 2004.
18. Muir, J.F.T., A. A., *Experimental investigation of the effects of nose bluntness, freestream Reynolds number, and angle of attack on cone boundary layer transition at a Mach number of 6.* AIAA Paper 72-216, 1972.
19. Stainback, P.C., *EFFECT OF UNIT REYNOLDS NUMBER, NOSE BLUNTNESS, ANGLE OF ATTACK, AND ROUGHNESS ON TRANSITION ON A 5" HALF-ANGLE CONE AT MACH 8.* NASA TN D-4916, 1969: p. 1-79.
20. Boudreau, A.H., *Transition measurements via heat-transfer instrumentation on a 0.5 bluntness 9.75-deg. cone at Mach 7 with and without mass addition.* AIAA Paper 85-1004, 1985: p. 1-7.
21. Fischer, M.C., *An experimental investigation of boundary-layer transition on a 10-deg. half-angle cone at Mach 6.9.* Technical Report NASA TN-D-5766, 1970: p. 1-63.
22. Horvath, T.J.B., S. A.; Hollis, B. R.,; Chang, C.-L.; Singer, B. A., *Boundary layer transition on slender cones in conventional and low disturbance Mach 6 wind tunnels.* AIAA Paper 2002-2743, 2002: p. 1-23.
23. Diaconis, N.S.J., J. R.; Wisniewski, *Boundary-Layer Transition at Mach 3.12 as Affected by Cooling and Nose Blunting.* NACA TN-3928, 1957: p. 1-17.
24. Rogers, R.H., *The Effect of Tip Bluntness on Boundary-Layer Transition on a 15 Deg Included Angle Cone at M = 3.12 and 3.81.* MINISTRY OF AVIATION AERONAUKAl RESEARCU COUNCIL CURRENT PAPERS, 1962. C.P. No. 598: p. 1-44.
25. Disher, J.H.R., L., *Observation of Laminar Flow on a Blunted 15 Deg Cone-Cylinder in Free Flight at High Reynolds Numbers and Free-Stream Mach Number to 8.17.* NACA RM E56G23, 1956: p. 1-33.
26. Stetson, K.F., Thompson, E. R., Donaldson, J. C., and Siler, L. G., *Laminar Boundary Layer Stability Experiments on a Cone at Mach 8, Part 4: On Unit Reynolds Number and Environmental Effects.* 1986. AIAA Paper 86-1087.
27. Zhong, X., *Effect of Nose Bluntness on Hypersonic Boundary Layer Receptivity over a Blunt Cone.* AIAA paper 2005-5022, 2005.
28. Zhong, X., *High-Order Finite-Difference Schemes for Numerical Simulation of Hypersonic Boundary-Layer Transition.* Journal of Computational Physics, 1998. 144: p. 662-709.
29. Zhong, X., and Ma, Y., *Boundary-layer receptivity of Mach 7.99 Flow over a blunt cone to free-stream acoustic waves.* Journal of Fluid Mechanics, 2005. 556: p. 55-103.
30. Zhong,X., "*Direct Numerical Simulation of Hypersonic Boundary-Layer Transition over Blunt Leading Edge, Part I : New Numerical Method and Validation (Invited),*" AIAA paper 97-0755,1997

31. Zhong,X., *Direct Numerical Simulation of Hypersonic Boundary-Layer Transition over Blunt Leading Edge, Part II : Receptivity to sound (Invited)*, AIAA paper 97-0756,1997.
32. Dietz, G. and Hein, S., *Entropy-layer instabilities over a blunted flat plate in supersonic flow*. Physics of Fluids, Volume 11, No.1, Jan 1999
33. Zhong,X., *Numerical Simulation of Hypersonic Boundary Layer Receptivity and Stability on Blunt Circular Cones,* AIAA paper 2009-0940, 2009.

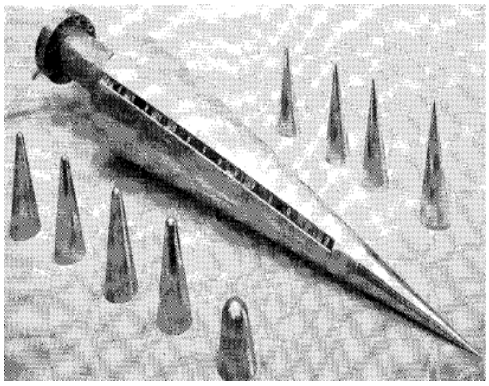

Figure 1. Sharp and blunt cones with an 8 degree half angle used in Stetson's transition experiments in a Mach 5.5 shock tunnel [3].

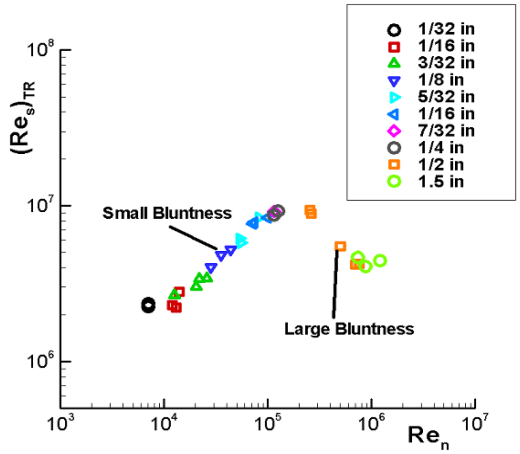

Figure 2. Free-stream transition Reynolds number vs. Reynolds number based on nose radius for Stetson's Mach 5.5 experiments (from Table 2 of [3]).

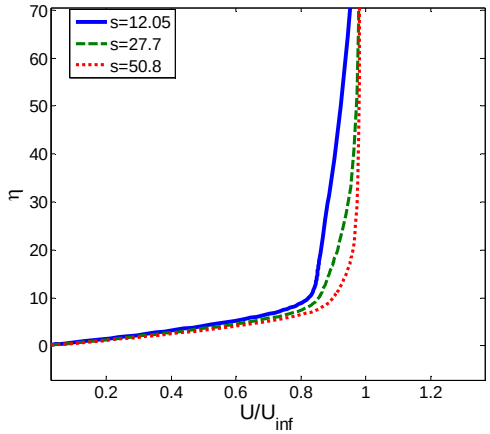

Figure 3. Non-dimensional U velocity profiles at different surface locations, case 2, r=3.969mm

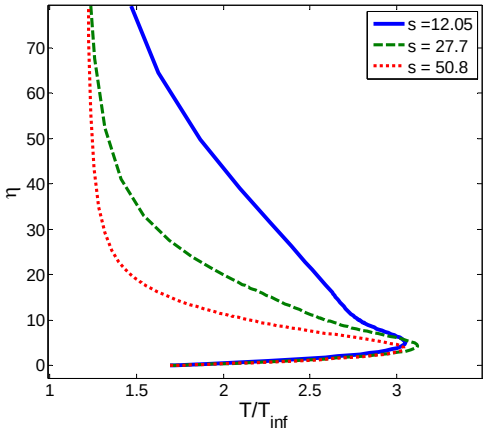

Figure 4. Non-dimensional temperature profiles at different surface locations, case 2, r=3.969mm

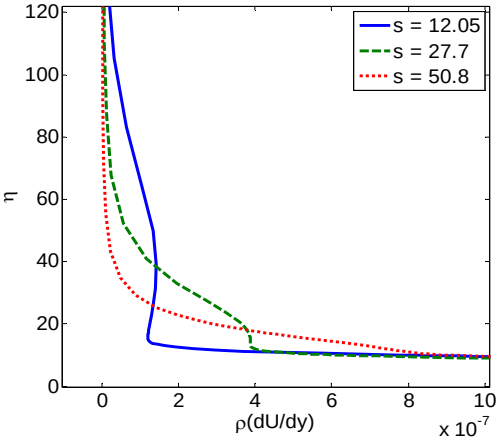

Figure 5. Non-dimensional $\rho\partial u/\partial y$ distributions at different surface locations, case 2, r=3.969mm

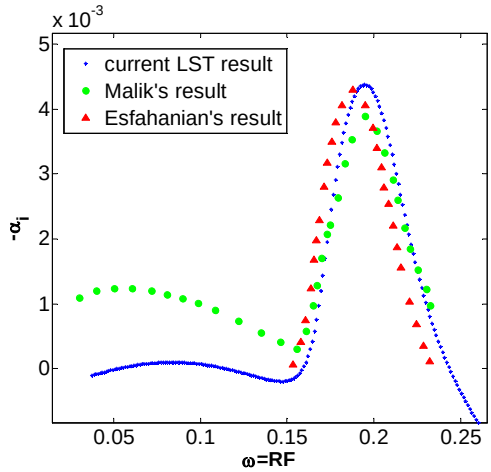

Figure 6. Growth rates of Mack modes for case 1 with r_n3.81mm at s=175

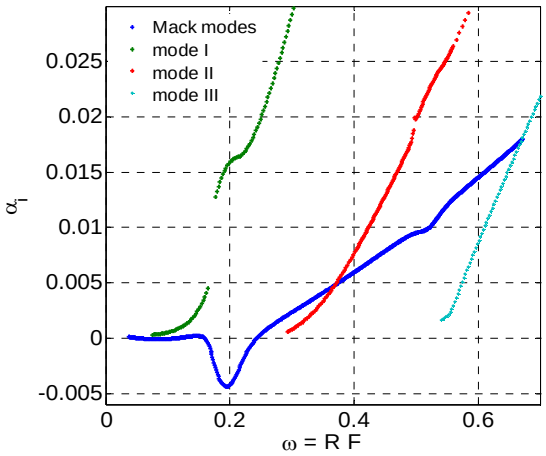

Figure 7. Growth rates of different normal modes for case 1 with r_n=3.81mm at s=175

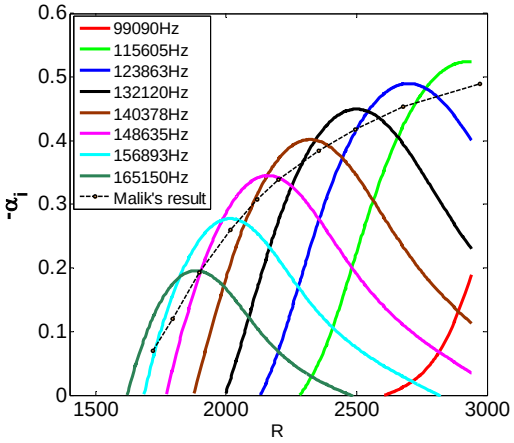

Figure 10. Second mode non-dimensional growth rates for case 1 with r_n=3.81mm

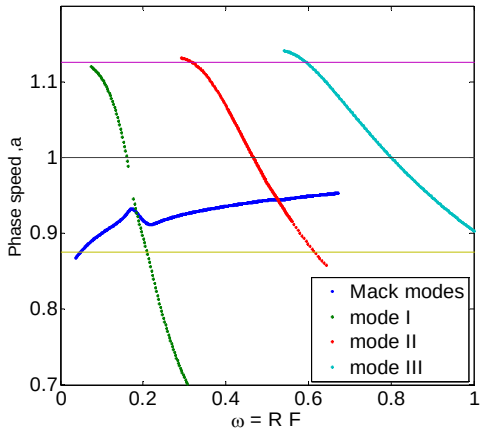

Figure 8. Phase speed of different normal modes for case 1 with r_n=3.81mm at s=175

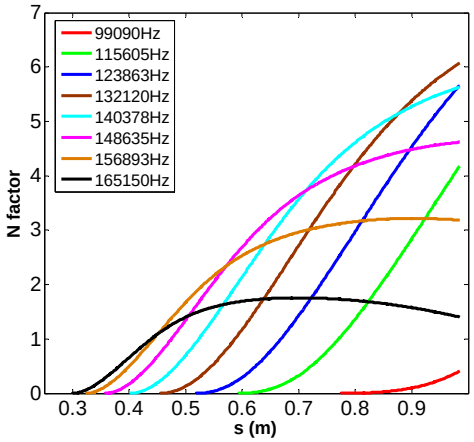

Figure 11. Second modes N factors for case 1 with r_n=3.81mm

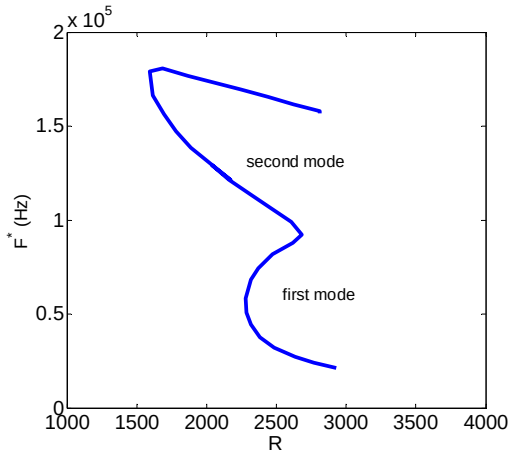

Figure 9. Neutral stability curve for case 1 with r_n=3.81 mm

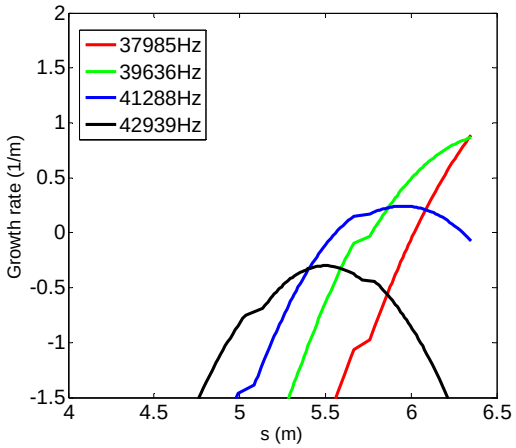

Figure 12. Second mode dimensional growth rates for case 1 with r_n=42.67mm

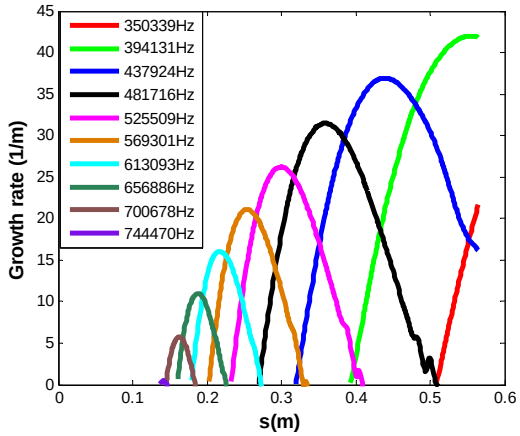

Figure 13. Second mode dimensional growth rates for case 2 with r_n=3.969mm

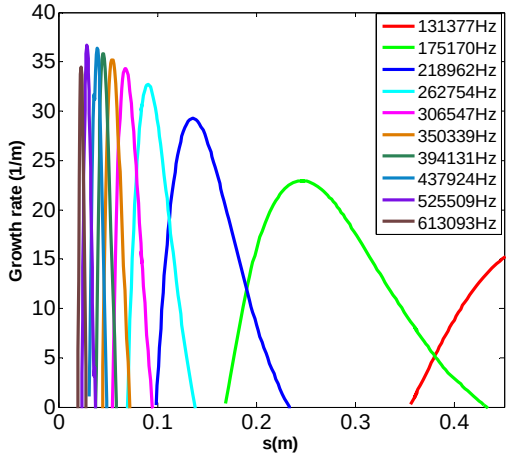

Figure 14. Second mode dimensional growth rate for case 2 with r_n=12.7mm

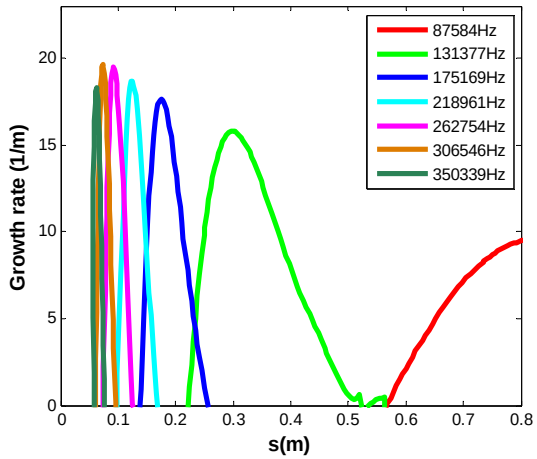

Figure 15. Second mode dimensional growth rate for case 2 with r_n=38.1mm

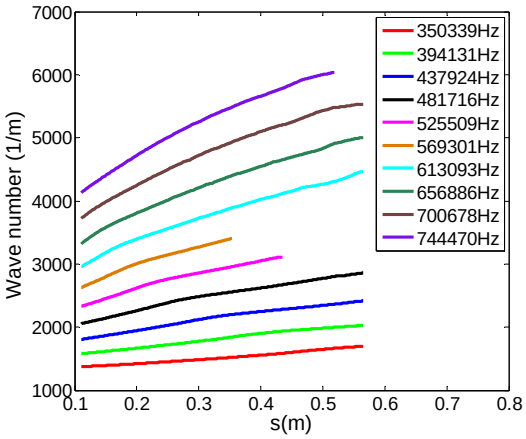

Figure 16. Second Mode dimensional wave number for Case 2 with r_n=3.969 mm

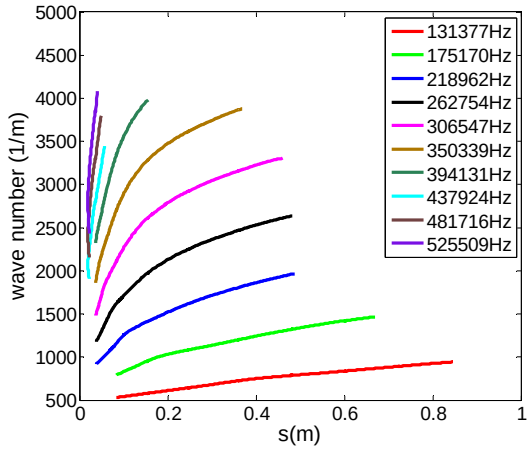

Figure 17. Second mode dimensional wave number for case 2 with r_n=12.7mm

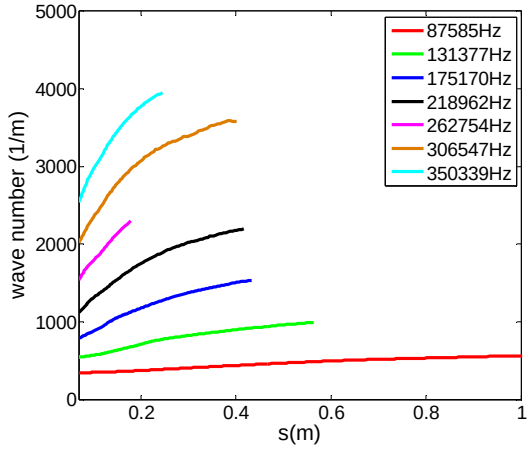

Figure 18. Second Mode dimensional wave number for Case 2 with r_n=38.1mm

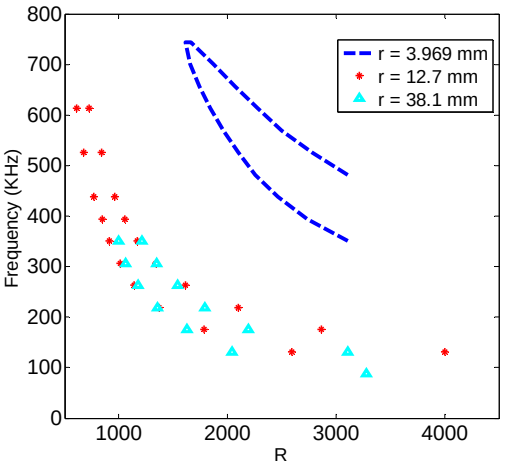

Figure 19. Second mode neutral stability lines for different nose bluntness of Case 2

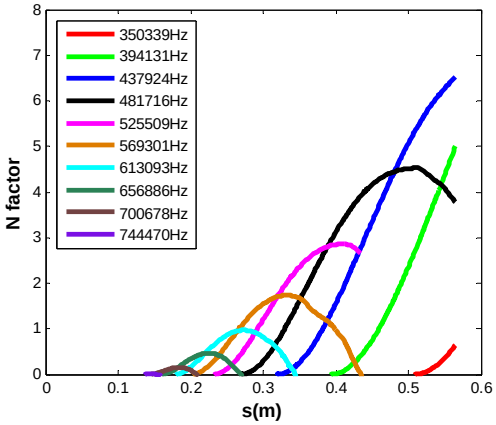

Figure 20. Second Mode N factor for Case 2 with r_n=3.969mm

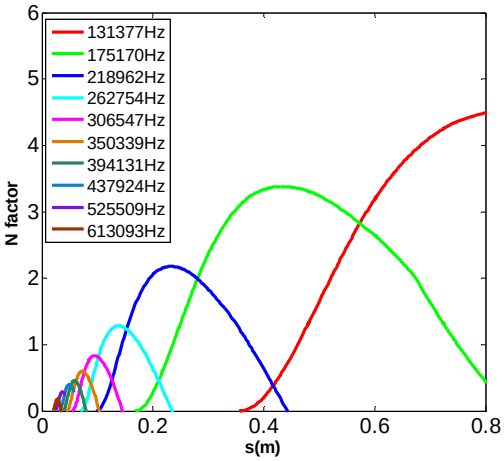

Figure 21. Second Mode N factor for Case 2 with r_n=12.7mm

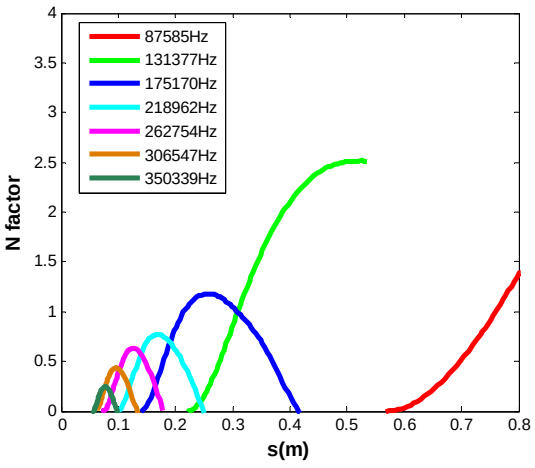

Figure 22. Second Mode N factor for Case 2 with r_n=38.1mm

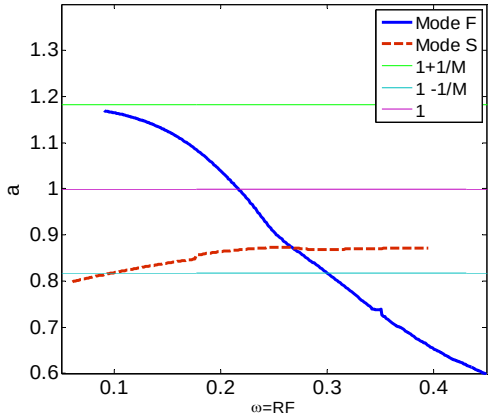

Figure 23. Phase speeds of mode F and mode S at s=120 (0.4763 m), case2, r=3.969 mm

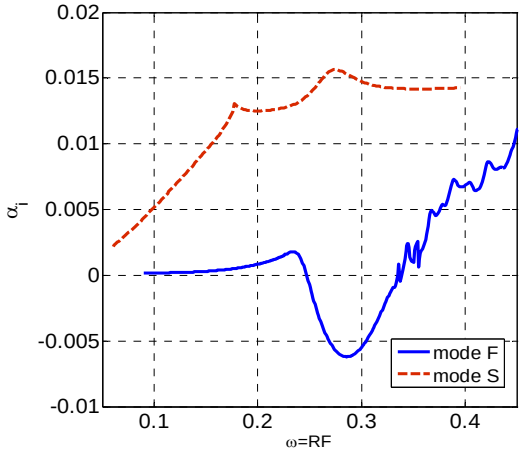

Figure 24. Non-dimensional growth rates of mode F and mode S at s=120 (0.4763 m), case2, r=3.969 mm

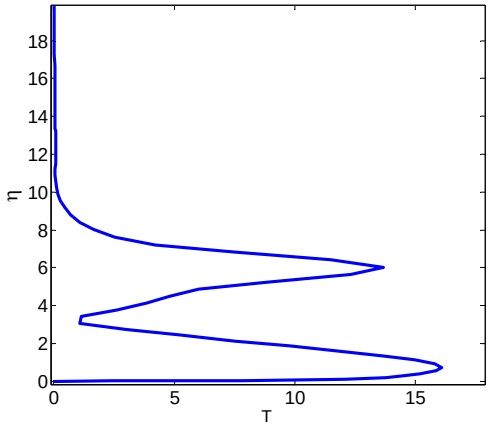

Figure 25. Temperature eigenfunction of second mode at synchronization, case 2, r=3.969 mm

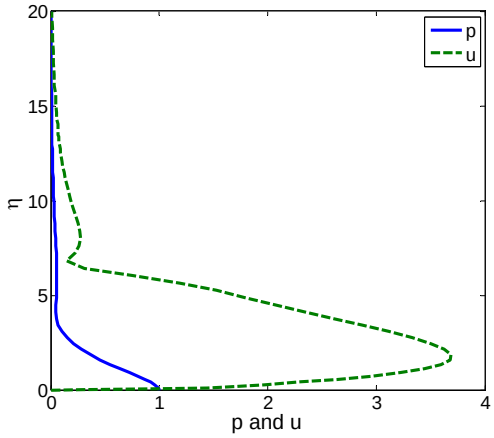

Figure 26. Pressure and u velocity eigenfunction of second mode at synchronization, case 2, r=3.969 mm